Leading-Edge Vortices Due to Low Reynolds Number Flow Past a Pitching Delta Wing

Rasheed Atta* and Donald Rockwell†
Lehigh University, Bethlehem, Pennsylvania

Flow past a pitching delta wing is examined in a water channel for a range of mean angle of attack. The wing is perturbed sinusoidally over a tenfold range of reduced frequency, in order to determine the nature of the vortex development and breakdown. There occur two basic types of vortex development: at low frequencies, the vortex core develops in the upstream direction towards the apex; at high frequencies, there is ejection of the leading edge of the vortex core from the apex in the downstream direction. Correspondingly, the direction of the dynamic hysteresis loop of vortex breakdown location vs angle of attack is determined by the type of vortex development. During unsteady development of the vortex core, the axial velocity on the centerline of the vortex is essentially constant with distance along the core. At the onset of vortex breakdown, there is abrupt deceleration; the velocity variations in this region exhibit a similar form for a range of angle of attack and reduced frequency.

Nomenclature

C	= chord
f_e	= excitation frequency
K	= reduced frequency $= \pi f_e C/U_\infty$
$L_{x'}$	= streamwise extent of deceleration along centerline of vortex core
P	= pitch of helical streamline
Re	= Reynolds number $= U_\infty C/\nu$
r	= radius of helical streamline
U_∞	= freestream velocity
u	= axial velocity of leading-edge vortex
u_c	= axial velocity on centerline of vortex
$(u_c)_{max}$	= maximum value of axial velocity on centerline of vortex
v_θ	= swirl velocity of vortex
x	= distance from apex of wing along centerline of vortex core
x_b	= distance of vortex breakdown from apex along centerline of core
x'	= distance along centerline of vortex core from onset of deceleration
$\bar{x}_p$	= distance from apex along leading edge of wing to location of wire probe
$\bar{x}_R$	= reference location along leading edge of wing for evaluating parameters of vortex
α	= angle of attack
$\bar{\alpha}$	= mean angle of attack
λ_e	= effective wavelength $= U_\infty/f_e$
ϕ	= swirl angle $= \tan^{-1} V_\theta/u$
ϕ_{max}	= maximum value of swirl angle
θ	= angular deflection of helical streamline pattern
ν	= kinematic viscosity

I. Introduction

THE structure of flow past a stationary delta wing has been studied extensively over the past few decades. Early investigations established that flow separation from the leading edge gives rise to a spiral-like vortex sheet on the upper surface of the wing; the consequence of this vortex pattern is an increase in lift, above that which would occur without leading-edge separation.[1-3] The study of Kuechemann,[4] which involves a nonlinear lifting-surface theory, describes this effect. More recent investigations[5-8] delineate details of the primary-secondary vortex system adjacent to the leading edge of the corresponding separation and reattachment lines.

The unsteady flow structure on a delta wing subjected to controlled motion has received less attention. The investigation of Lambourne et al.[9] demonstrated the concept of phase shift between development of the vortex pattern at a given cross section and the stepwise motion of the wing in the plunging mode. For the case of simple harmonic motion in the pitching mode, Gad-el-Hak and Ho[10] observed an analogous phase shift of the growth-decay cycle of the cross sections of the leading-edge vortices. This phase shift, or hysteresis, during the course of the wing oscillation cycle was characterized in terms of height or thickness of the dye marking the vortex; the degree of hysteresis was found to be a strong function of reduced frequency. Further aspects of the unsteady three-dimensional structure on various wings are addressed in the subsequent investigations of Gad-el-Hak and Ho.[10,11] They emphasize the importance of mutual induction between leading- and trailing-edge vortices in determining the overall flow structure.

Central to the unsteady structure of the leading-edge vortices is the time-dependent development of the vortex core along its streamwise extent and its eventual breakdown. This breakdown is characterized by abrupt transition from a jet-like to a wake-like core of the vortex, accompanied by a substantial increase in turbulence activity. It has been investigated for flow past a variety of stationary wing configurations, as reviewed by Wedemeyer.[12] For sinusoidal wing motion at high reduced frequency, Atta and Rockwell[13] observed occurrence of the maximum breakdown position of the core near the maximum angle of attack, rather than at the minimum angle of attack expected from the quasisteady considerations; and existence of the vortex core over only a fraction of the oscillation cycle.

An insightful framework for study of vortex breakdown is provided by the extensive investigations of internal flows in tubes as, for example, described by Sarpkaya,[14] Garg and Leibovich,[15] and Escudier.[16] These, as well as other experimental studies, and a wide range of theoretical approaches beyond the scope of this introduction, are incisively assessed by Leibovich.[17,18] In essence, the investigations of vortex

Received July 21, 1988; revision received Jan. 19, 1989.

*Graduate Student; presently Professor of Engineering and Technology, Minia University, Minia, Egypt.

†Paul B. Reinhold, Professor, Department of Mechanical Engineering and Mechanics. Member AIAA.

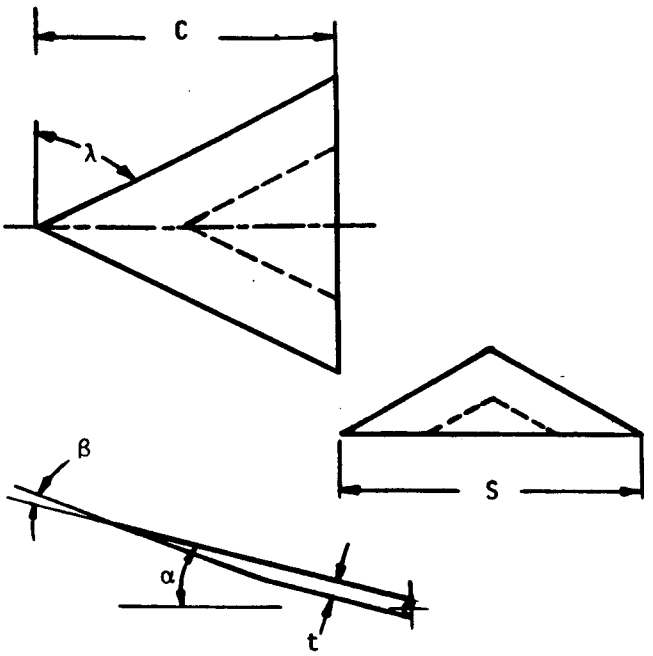

Fig. 1 Schematic of delta wing.

breakdown addressed therein focused on steady inflow conditions. Exceptions include the investigations of Lambourne,[19] Sarpkaya,[20] and Faler and Leibovich,[21] who reveal interesting aspects of transient vortex development and overshoot of the vortex breakdown position.

There are a number of unexplored issues related to the unsteady vortex development and breakdown on an oscillating delta wing: the classes of unsteady development of the vortex core in the vicinity of the apex of the wing; the possible mechanisms of vortex breakdown; the types of dynamic hysteresis of the instantaneous breakdown position relative to the instantaneous angle of attack; the core flow structure associated with these types of hysteresis; the nature of secondary vortex development and breakdown relative to its primary vortex counterpart; and variations in velocity of the vortex core during the wing oscillation cycle. In the following, we address these issues.

II. Experimental Systems and Techniques

All experiments were carried out in a water channel with a removable test section that supported the oscillating delta wing arrangement, described in detail by Atta.[22] The test section insert had an internal width of 254 mm, a height of 457 mm, and a length of 457 mm. The delta wing was supported at its trailing edge by either a taut wire having a diameter of 0.8 mm or a small rod of diameter 3.2 mm; cross comparison showed that both arrangements gave the same results for the parameters of interest herein. The driving mechanism for forcing the wing sinusoidally about its trailing edge was mounted on a steel frame above the channel. The main part of the forcing mechanism was a motor-pulley-cam system. The eccentric cam was located on a large pulley which, in turn, supported a nominally horizontal lever arm. This forcing system was driven by a continuous duty dc motor. The connection from the forcing system to the pitching axis of the wing was a vertical rod with sharp ends, providing a needle bearing connection at either end of the rod. This rod was located exterior to the test section insert in order to preclude interference effects. A complete description of the forcing system is given by Atta.[22]

In order to allow examination of the flow structure over a range of Reynolds number using different visualization techniques, wings of several different scales were employed. All wings were geometrically similar (see Fig. 1), having a sweep angle $\lambda = 52$ deg. All were milled flat on one side, and at a bevel angle of $\beta = 10$ deg on the other side. The chord C of the wings investigated was $C = 51$, 76, and 102 mm. Using these wings, it was possible to examine the principal features of vortex development and breakdown over a range of Reynolds number. All hydrogen bubble visualization shown and analyzed herein for the stationary wings was at $Re = 5800$. Dye visualization excerpts for the pitching wing fall in the range $2900 \leq Re \leq 5800$, and hydrogen bubble excerpts in the range $2900 \leq Re \leq 13{,}400$.

Two visualization techniques were employed: dye injection and hydrogen bubble methods. Dye injection was from holes at two different locations. The first location was positioned a distance of 3.2 mm from the apex in the slanted edge of the wing. The second location was also a distance of 3.2 mm from the apex, but in the flat surface coincident with a line passing through the apex and making an angle of 27 deg with the wing centerline. In essence, the same flow structure was observed irrespective of the dye hole location, the important point being that the dye must be continually injected into the core of the vortex at or near the apex throughout the oscillation cycle.

For the hydrogen bubble technique, a 25-μm wire was mounted on moving supports located well away from the wing, which were fixed to the pitching axis of the wing; this arrangement allowed the wire stretched (at an angle) across the apex to rotate at the same tip velocity as the apex. Full details of this intricate flying wire arrangement are given by Atta.[22] Cross comparison of the time-dependent core structure using these techniques and the foregoing dye method showed indistinguishable results.

To illuminate the flowfield, stroboscopic lighting was employed; it was synchronized with the main frame of the video system and with the video cameras. Instar strobes having an output of 90 W at a frequency of 120 Hz were used to illuminate the region of interest. The stroboscopic lights were directed at an oblique angle to the line of sight of the camera in order to secure the best contrast in the recordings. The strobes were adjusted to relatively small angles from the line of sight of the camera for close-up views where low light intensity was required. On the other hand, they were adjusted to larger angles for overview (long distance) cases that required higher light intensity. An alternate technique of illumination involved a laser sheet produced by steering a 2-W Argon-ion laser beam to a rotating mirror oscillating at 500 cps. This laser sheet, oriented orthogonal to the axis of the vortex, illuminated the desired cross section of the vortex flow. It provided a detailed end view, which complemented that obtained from diffuse lighting.

The flow visualization was recorded with a high-speed (120 frames/s) video system manufactured by Video Logic Corporation. Images were recorded on 1-in. magnetic tape, allowing slow motion and frame-by-frame analysis. Hard copies of the video images were obtained by photographing the video screen in the still-frame mode with a 35 mm Nikon FN camera.

III. Vortex Breakdown on Stationary Wing

The location of vortex breakdown in the stationary wing and the variation of centerline velocity of the vortex core were characterized in detail for angles of attack $5 \text{ deg} \leq \alpha \leq 20$ deg.[22] Data from this investigation agree well with that from other related studies extending up to $Re = 10^6$, as surveyed by Atta.[22] At $\alpha = 20$ deg, vortex breakdown occurred at the apex of the wing, and at $\alpha = 10$ deg, it was located at the trailing-edge of the wing.

A distinguishing feature of vortex formation from the leading-edge of a delta wing, relative to the extensively investigated case of internal flow in tubes, is that velocity is continuously fed into the core of the vortex as it evolves along the edge of the wing. The effective radius of the vortex core increases with distance along the edge, producing departures from the simplified columnar vortex flow. The swirl angle ϕ of the vortex is defined as $\phi = \tan^{-1} v_\theta/u$, in which v_θ and u are the swirl and axial velocities, respectively. In order to deter-

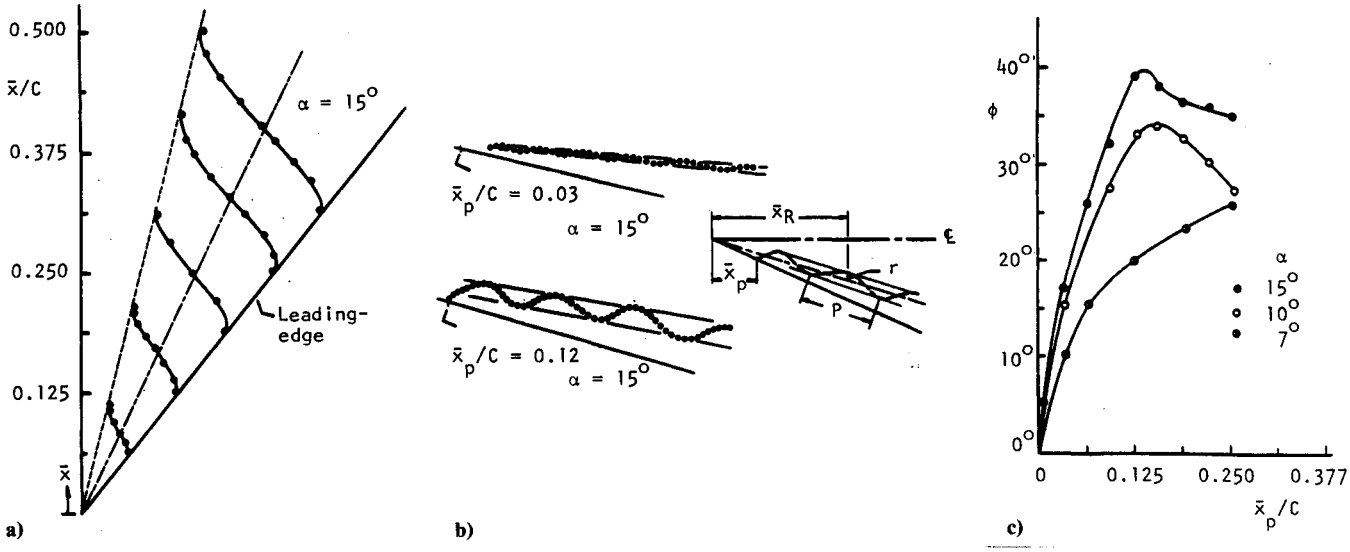

Fig. 2 a) Plan view of initial portions of streamlines emanating from leading edge of wing determined by laser-sheet technique; b) side view of representative helical streamline patterns; and c) swirl-angle distribution as a function of distance along leading edge.

mine the swirl angle ϕ and the streamlines, two basic techniques were employed. In the first method, a laser sheet, whose plane was orthogonal to the axis of the vortex, was employed to examine successive slices of the vortex cross section. To mark the flow, a platinum wire (25 μm) probe for generating hydrogen bubbles was placed against the leading edge at location $\bar{x}_p$ from the apex of the wing. Distortions of the bubble pattern allowed tracking the trajectory of the streamline emanating from location $\bar{x}_p$. The second method involved similar placement of a wire along the edge at location $\bar{x}_p$. In this case, the helical pattern of the vortex was clearly evident from the side view. Consequently, it was possible to determine incremental changes in pitch P and angular deflection θ of the helix at a given radius r. In both of the foregoing methods, placement of the marker probe at a location $\bar{x}_p$ near the apex marked the innermost portion of the core, while locating it well downstream of the apex produced helical patterns in the outermost region of the core.

Figure 2a shows a plan view of a typical streamline pattern from the laser-sheet method. The data points intersecting the leading edge of the wing represent locations $\bar{x}_p$ of the marker probe. Figure 2b shows side views of the helix visualized with the marker probe at $\bar{x}_p$ using the diffuse-lighting technique. These helical patterns are representative of a large number of them acquired for angles of attack $\alpha = 7$, 10, and 15 deg. Close examination of the patterns of Fig. 2b shows that their pitch, as well as radii, increase with distance along the vortex.

The swirl angle ϕ at a reference location $\bar{x}_R/C = 0.375$ was determined by evaluating the incremental pitch and angular displacement of the helix from the side view at the reference location $\bar{x}_R$, while moving the marker probe to successive locations $\bar{x}_p$ along the edge of the wing, as illustrated in Fig. 2c. For $\alpha = 10$ and 15 deg, $\phi_{max} = 33$ and 39 deg. Comparing these values of ϕ_{max} with vortex breakdown locations given by Atta,[22] we note that vortex breakdown moves upstream with increasing α, which generates increasing ϕ_{max}. It occurs at $x/C = 1.07$, 1.0, and 0.43 for $\alpha = 7$, 10, and 15 deg. Transformation of the ϕ vs $\bar{x}_p$ distributions of Fig. 2c to ϕ vs r, where r is the radius from the center of the vortex, was done by determining nonlinear variations of r vs $\bar{x}_p$. From these ϕ vs r distributions, at $\alpha = 10$ and 15 deg, $\phi_{max} = 37.5$ and 41 deg.

For all values of parameters investigated herein, the vortex breakdown was in the spiral mode, in contrast to the bubble (quasiaxisymmetric) mode. It is appropriate to compare the values of maximum swirl angle with those obtained for spiral vortex breakdown in internal (tube) flows, where the approach flow is constrained to be axisymmetric and distortions (to be

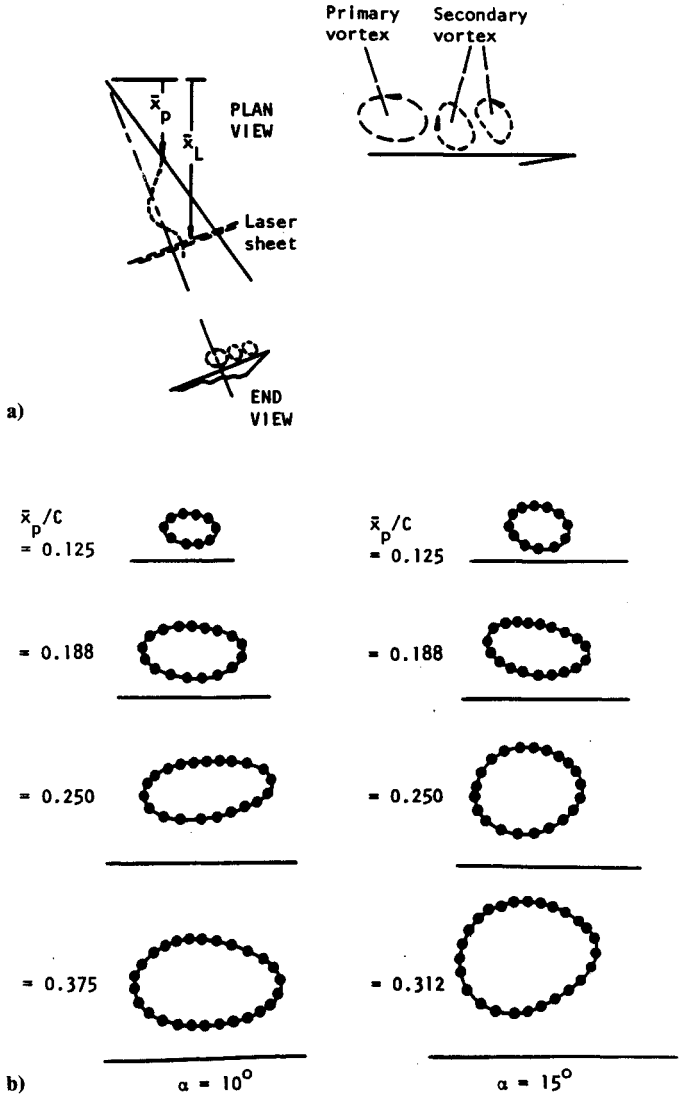

Fig. 3 a) Typical cross section of vortex structure showing primary and secondary vortices; and b) variation of shape and orientation of primary vortex core as a function of distance from apex of wing. Contours with dots represent completion of first revolution of helical streamline emanating from marker probe at location $\bar{x}_p$.

shown in Fig. 3) are not present. Garg and Leibovich[15] found 43.8 deg $\leq \phi_{max} \leq$ 46.0 deg for the spiral mode and 49.7 deg $\leq \phi_{max} \leq$ 52.2 deg for the bubble mode. Sarpkaya[20] observed 38 deg $\leq \phi_{max} \leq$ 55 deg for the spiral mode and $\phi_{max} \approx$ 50 deg for the bubble mode. The present values of ϕ_{max} for spiral mode breakdown on the delta wing (given in the foregoing) are near the lower value of the range of ϕ_{max} for spiral mode breakdown in tube flow. Moreover, the present values of ϕ_{max}, for which no bubble mode could be detected, are below those values for which the bubble mode of breakdown occurred in the flow.

In the foregoing, attention has been focused on the character of the primary (major) vortex formed from the leading edge of the wing. The full complexity of the vortex development is illustrated in Fig. 3. Using the laser-sheet technique, it is possible to visualize not only the primary vortex addressed in the foregoing, but also the secondary vortices, schematically depicted in Fig. 3. The primary vortex is, of course, fed by vorticity from the boundary layer along the leading edge of the wing. The secondary vortex immediately adjacent to it, however, is fed by vorticity from the boundary layer on the surface of the wing. On the other hand, the secondary vortex immediately next to the edge of the wing is fed by that portion of vorticity from the edge of the wing that is peeled off from the separating shear layer feeding the primary vortex. All of these vortices are nonaxisymmetric. The plots of Fig. 3, taken at two different angles of attack $\alpha = 10$ and 15 deg, show a quasielliptical cross section of the primary vortex. Its orientation changes with streamwise distance. This tilting and distortion of the primary vortex is associated with the fact that the distance of its axis from the leading edge of the wing increases with streamwise distance; correspondingly, the nature of the secondary vortices is altered as well. Clearly, characterization of the aforementioned parameters for the primary vortex must be viewed in the context of the entire system of vortices in the vicinity of the leading edge.

IV. Vortex Development and Breakdown on Oscillating Wing

In defining the effects of unsteadiness induced by the wing motion, it is essential to determine the relationship between the instantaneous structure of the (primary) vortex core and the instantaneous position of the wing. Moreover, knowledge of the relationship between the development of the primary and secondary vortices is desirable.

A. Basic Classes of Vortex Development

When the wing is subjected to pitching motion at frequency f_e, the structure of the vortex core development and breakdown can be expected to be a strong function of the reduced frequency $K = \pi f_e C/U_\infty$. In essence, this dimensionless frequency represents the ratio of the wing chord C to the wavelength U_∞/f_e of the forced motion. Examination of the flow structure over the range of reduced frequency $0.025 \leq K \leq 1.7$ and mean angle of attack 5 deg $\leq \bar{\alpha} \leq$ 20 deg shows that there

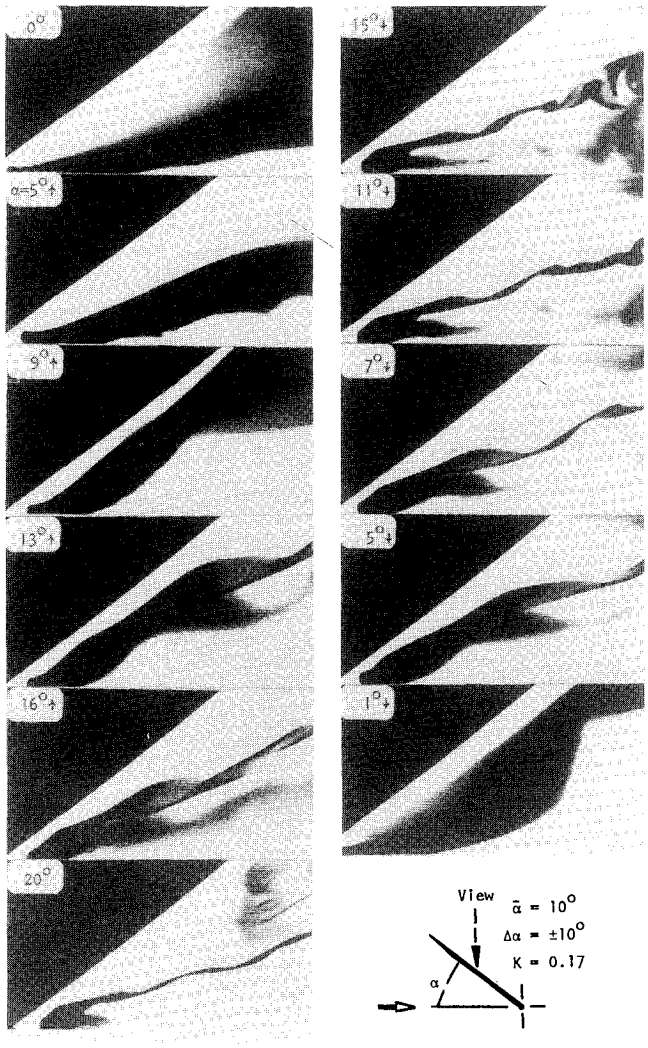

Fig. 4 Time sequence showing mechanisms of development and collapse of vortex core at low reduced frequency, visualized by dye injection near apex ($K = 0.17$).

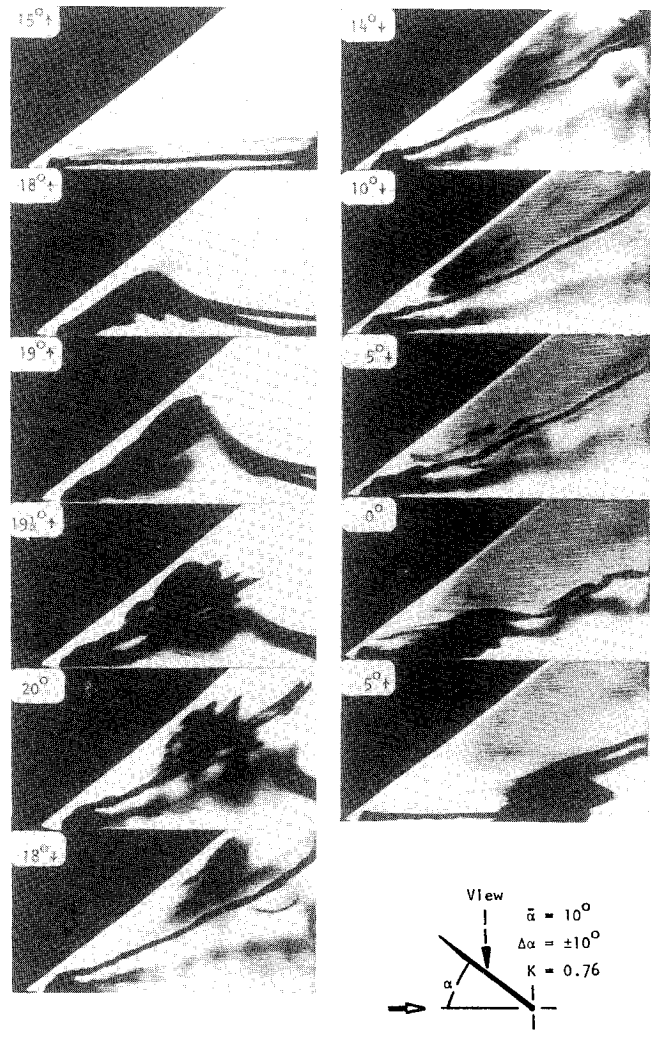

Fig. 5 Time sequence showing mechanisms of development and collapse of vortex core at high reduced frequency, visualized by dye injection near apex ($K = 0.76$).

are two fundamental types of vortex development during the course of an oscillation cycle. At low reduced frequencies, the development of the vortex core is as represented in Fig. 4; at higher reduced frequencies, it takes the form shown in Figs. 5 and 6. Further aspects of the flow structure are given in Fig. 7. For all visualization in Figs. 4–7, the field of view extends over the domain $0 \le x/C \le 0.5$.

For the case of relatively low reduced frequency represented in Fig. 4, the dye migrates along the surface of the wing towards the leading edge for $\alpha = 5$ deg ↑ and 9 deg ↑ (upward ↑ and downward ↓ arrows correspond to upstroke and downstroke motions, respectively). At $\alpha = 13$ deg ↑, there is evidence of onset of vortex core formation in the right portion of the photo. At $\alpha = 16$ deg ↑, this development progresses further until, at $\alpha = 20$ deg, the core is fully formed and has its maximum streamwise extent. This observation is in marked contrast to the case of the stationary wing for which vortex core breakdown occurs at the apex (Atta[22]). During the downstroke motion, at $\alpha = 15$ deg ↓, vortex breakdown in the spiral mode is evident. However, as shown in the photo corresponding to $\alpha = 11$ deg ↓, further upstream movement of this breakdown is inhibited by the collapse of the vortex core near the apex. This streamwise extent of the core collapse moves downstream successively at $\alpha = 7$ deg ↓, 5 deg ↓, until at $\alpha = 1$ deg ↓ there is no indication of a vortex core. At $\alpha = 0$ deg, the dye marker has moved towards the midplane of the wing. In essence, the foremost characteristic of this type of vortex development is that formation of the vortex core occurs first in the downstream region of the wing and moves upstream with increasing angle of attack; conversely, the collapse of the vortex moves in the downstream direction during the downstroke motion of the wing. Moreover, there is clearly a phase shift between the instantaneous flow structure and the instantaneous angle of attack. Because of this phase shift, the character of the vortex core at a given angle of attack is different during the upstroke and downstroke motion, evident by comparison of photos at $\alpha = 5$ deg ↑ and 5 deg ↓; and 13 deg ↑, 16 deg ↓, and 15 deg ↓. It is remarkable that there is such a substantial difference between the structure during the up and downstroke motion at this value of frequency $K = 0.17$, corresponding to a value of excitation wavelength $\lambda_e = U_\infty / f_e$ over an order of magnitude greater than the chord C of the wing.

At a sufficiently high value of reduced frequency, the development of the vortex core is markedly different than that illustrated in Fig. 4. As indicated in Fig. 5, from $\alpha = 15$ deg ↑ to $\alpha = 18$ deg ↑, the dye is abruptly swept towards the leading edge and in subsequent photos corresponding to $\alpha = 19$ deg ↑, 19.5 deg ↑, and 20 deg, there is eruption of the leading edge of the vortex core from this region of agglomerated dye. At $\alpha = 18$ deg ↓ through $\alpha = 10$ deg ↓, the integrity of the vortex core is maintained, while there is flow in the upstream direction between the leading edge of the wing and the vortex core; this upstream flow is clearly indicated by tracking the agglomeration of dye adjacent to the leading edge. At $\alpha = 5$ deg ↓ through $\alpha = 5$ deg ↑, there is progressive collapse of the vortex core downstream of the apex. In essence, the principal feature of this vortex development at higher frequencies is the rapid ejection of the leading edge of the vortex core, in the downstream direction, during the core formation process.

At very high reduced frequency, indicated in Fig. 6, the development of the vortex core is very similar to that of the preceding. There is rapid ejection of the leading edge of the core from the apex region. This is evident in photos corresponding to $\alpha = 15$ deg ↓ and 12 deg ↓. However, commencing with $\alpha = 8$ deg ↓ and proceeding through $\alpha = 3$ deg ↓, there is rapid development of a column-type instability of the vortex core; the classical spiral mode of instability is bypassed completely. At $\alpha = 0$ deg, the agglomeration of the dye corresponding to the column-type instability has moved downstream, and at $\alpha = 10$ deg ↑, the vortex core ceases to exist.

As shown in the foregoing, a remarkable consequence of this phase shift is occurrence of the maximum length of the vortex core (prior to breakdown) near or at the maximum instantaneous angle of attack of the wing (see $\alpha = 18$ deg ↓ photo in Fig. 5). At higher mean angle of attack, this effect can be even more striking, as evidenced in Fig. 7. In this case, the maximum length of the vortex core in the streamwise direction

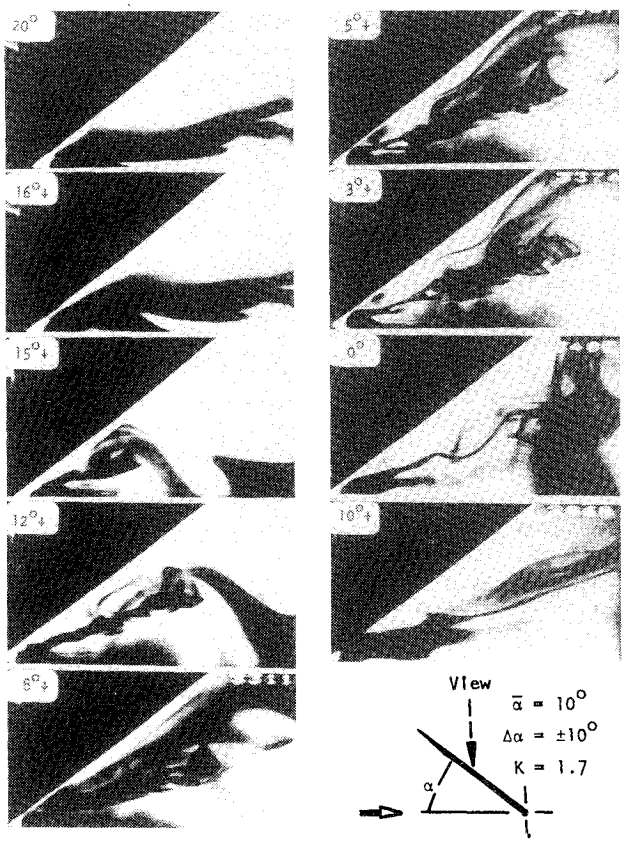

Fig. 6 Time sequence showing mechanisms of development and collapse of vortex core at very high reduced frequency, visualized by dye injection near apex ($K = 1.7$).

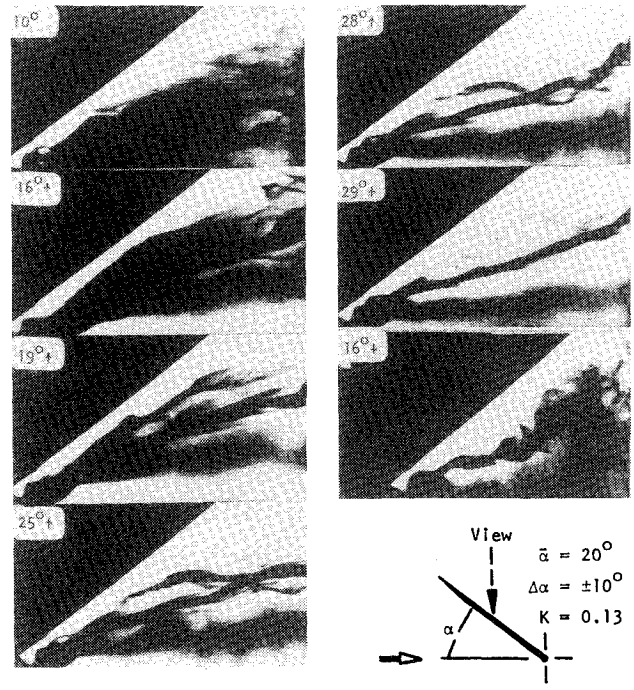

Fig. 7 Illustration of vortex core development and collapse at low reduced frequency $K = 0.13$ and high mean angle of attack $\bar{\alpha} = 20$ deg.

occurs at $\alpha = 29$ deg ↑; the stationary wing shows breakdown of the vortex core to occur at the apex of the wing at $\alpha = 20$ deg (see Atta[22]). The events leading to formation of this long vortex core show the same general trend as the representative low-frequency case given in Fig. 4: the vortex core develops from the downstream region of the flow in the upstream direction towards the apex for $\alpha = 10$ deg ↑ through $\alpha = 29$ deg ↑. Evident in the range of $\alpha = 19$ deg ↑ to 28 deg ↑ is the development and disappearance of the secondary vortex between the primary vortex and the leading edge of the wing. As will be addressed subsequently, such secondary vortex formation and decay always leads that of the corresponding primary vortex. During the downstroke motion, the length of the vortex core decreases, as represented by the photo $\alpha = 16$ deg ↓.

When the wing pitches about its trailing edge, the wing velocity will be maximum at the apex and zero at the trailing edge. Correspondingly, the effective angle of attack will vary with distance along the leading edge. Provided that the potential flow about the wing does not depart significantly from the quasisteady flow, one would expect that during pitch-up motion, the vorticity flux from the surface of the wing into the leading-edge vortex would decrease and for the pitch-down motion would increase. In other words, these respective motions of the wing would retard and augment the vortex-formation processes, with the largest effects occurring near the apex where the wing velocity is highest. However, this simplified interpretation is complicated by 1) the finite length of the vortex core, bounded at its upstream end by its origin at the apex and at its downstream end by vortex breakdown; and 2) the drastically different response times of the vortex core without and with occurrence of vortex breakdown, of the order of $C/U_\infty = 1$ and 10, respectively, for a constant pitching rate (Reynolds and Abtahi[23]). The coexistence of both of these time scales during a typical oscillation cycle precludes any simple interpretation on a quasisteady basis. In fact, at the lowest value of reduced frequency considered in the visualization series ($K = 0.17$ in Fig. 4), the maximum streamwise extent of the core before breakdown occurs at maximum angle of attack, in direct contrast to what occurs for the static wing.[22]

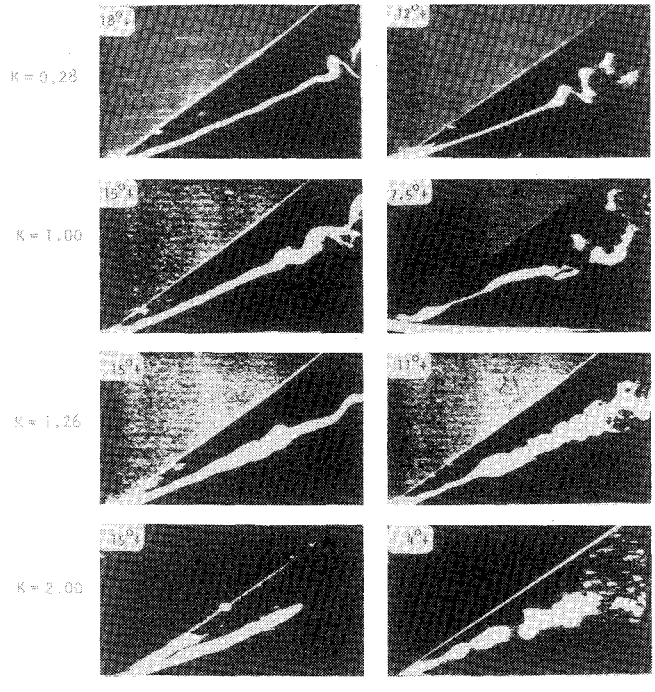

Fig. 8 Basic classes of vortex development and breakdown as a function of reduced frequency.

B. Basic Classes of Vortex Breakdown

In the foregoing cases, shown in Figs. 4–7, the general features of low- and high-frequency vortex development were illustrated. The focus of these studies was on the vortex development on the upstream portion of the wing. Extensive study of flow-visualization films covering a greater fraction of the wing chord $0 \le x/C \le 0.8$, and over a wider range of reduced frequency $0.25 \le K \le 1.7$ for mean angle of attack 5 deg $\le \bar{\alpha} \le$ 35 deg, showed several classes of vortex breakdown, as given in Fig. 8. In each case, the core development is shown at two successive instants of time. The hydrogen-bubble technique was used for visualization by mounting a flying wire at the apex of the wing, as described in Sec. II. Subsequently, these patterns were verified using dye injection. At sufficiently low values of reduced frequency, the breakdown of the vortex core was in the classical spiral mode, as observed on the stationary wing. This is represented in Fig. 8 corresponding to $K = 0.28$. At higher reduced frequency, there can occur a large-scale spiral mode, represented by the case $K = 1.0$. Therein, the classical spiral instability shown for $\alpha = 15$ deg ↓ is abruptly overshadowed by a large-scale spiral mode having substantially longer wavelength and larger characteristic diameter at $\alpha = 7.5$ deg ↓. At $K = 1.26$, there occurs a column-type instability; this instability is characterized by a sudden thickening in diameter of the vortex core. It preempts the classical spiral instability occurring at the right portion of the photo. At $\alpha = 11$ deg ↓, this column-type instability is shown to dominate the entire breakdown of the vortex. Finally, at high reduced frequency, represented by the case $K = 2.0$, the column-type instability near the apex produces immediate and simultaneous destruction of the organized core, evidenced by the sequence at $\alpha = 15$ deg ↓ and 4 deg ↓.

C. Dynamic Hysteresis of Development and Breakdown of Core Primary Vortex

In the preceding section, the basic types of low- and high-frequency vortex development and breakdown were defined. A principal observation was the phase shift between the instantaneous structure of the vortex core and the instantaneous wing motion, relative to what occurs for the stationary wing. A means of quantitatively expressing this phase shift is to plot the instantaneous breakdown position x_b, i.e., the distance of occurrence of vortex breakdown from the apex of the wing, against the instantaneous angle of attack α.

As shown in Fig. 9, such plots take the form of dynamic hysteresis loops. Both the shape of the loop and its direction, i.e., either clockwise or counterclockwise, are predominantly functions of reduced frequency K, evidenced by studies over the ranges of parameters given in Sec. IVA. The top plot of Fig. 9 shows, as a reference, the x_b/C vs α characteristic for the case of a stationary wing; in this case, vortex breakdown occurs at the apex at an angle of attack $\alpha = 20$ deg. Also shown on the same set of axes is the hysteresis loop for a low value of reduced frequency $K = 0.025$. There is indeed substantial hysteresis, in that the value of x_b at a given angle of attack α strongly depends upon whether the downstroke or upstroke motion is considered. The general trend of this hysteresis loop and its clockwise sense (i.e., direction of rotation) are maintained for $K = 0.05$ and $K = 0.13$. The corresponding development of the vortex core is in the upstream direction towards the apex, as illustrated in Fig. 4.

At a higher value of reduced frequency $K = 0.28$, the loop tends toward a figure-eight form. It is characterized by gradual appearance and stabilization of the vortex core on the upstroke. After the core is established, vortex breakdown occurs in the usual fashion, but is drastically shifted in phase with respect to the case of the stationary wing. For all cases through $K = 0.28$, this vortex core breakdown occurs in the classical spiral mode, as indicated schematically on each of the plots of x_b/C vs α.

At still higher values of reduced frequency, $K = 0.76$ and 1.6, there is a drastic change in the form of the hysteresis loop.

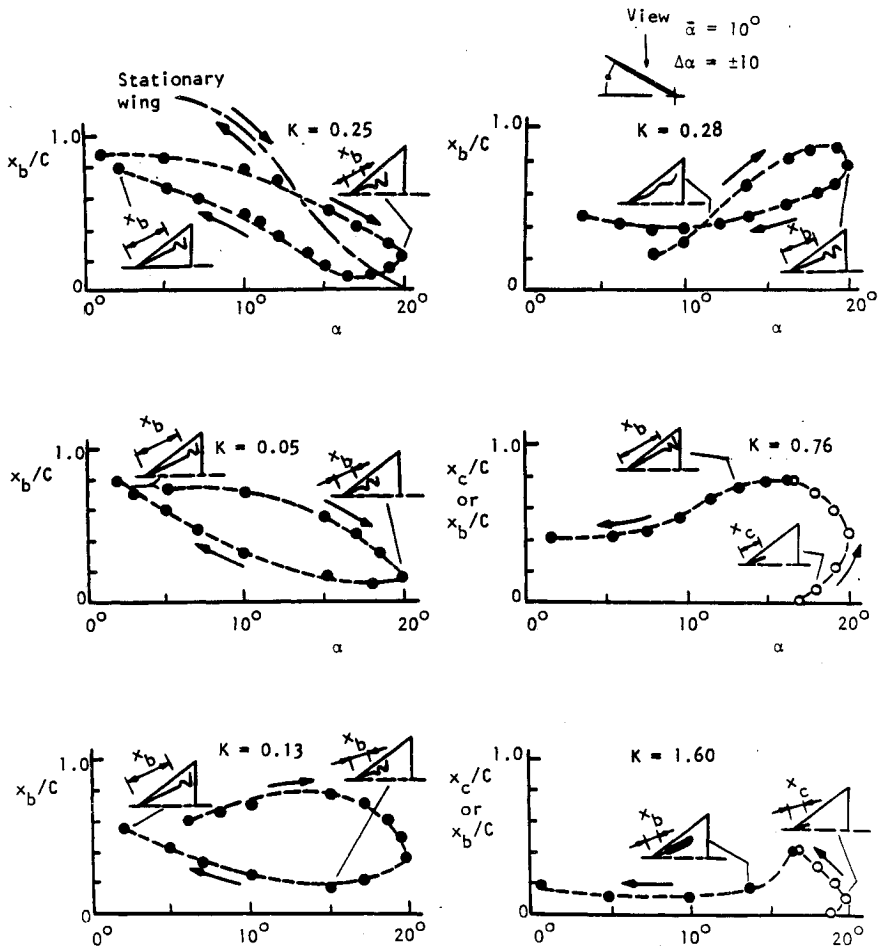

Fig. 9 Comparison of dynamic hysteresis loops of vortex development and breakdown as a function of reduced frequency.

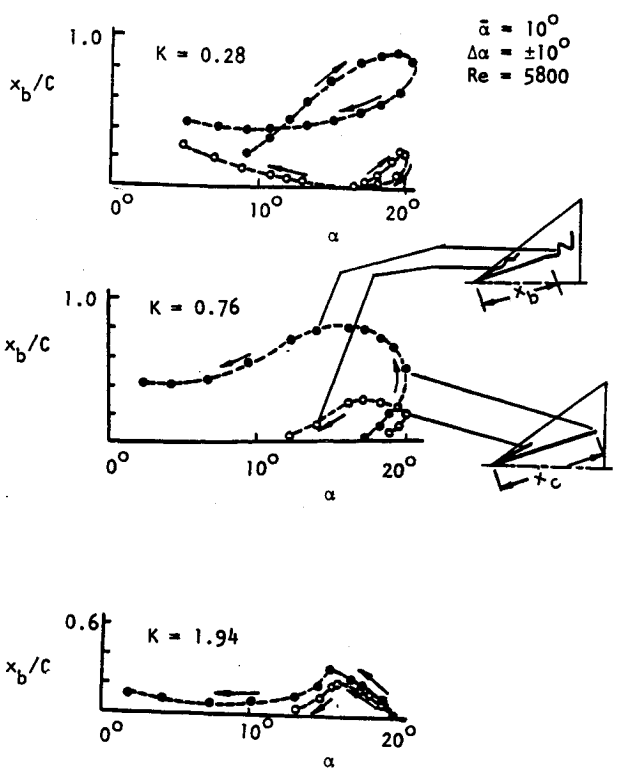

Fig. 10 Comparison of dynamic hysteresis loop for primary (closed symbol) and secondary (open symbol) vortex development.

The sense of the loop is now in the counterclockwise direction. These changes in the form and direction of the loop are due to the onset of ejection of the leading edge of the vortex core from the apex region (see Figs. 5 and 6). At these high values of K, the vortex core does not exist over a substantial part of the wing cycle, i.e., for 0 deg $\leq\alpha\leq$ 17 deg at $K=0.76$ and 0 deg $\leq\alpha\leq$ 18.5 deg at $K=1.6$. When the vortex core does appear by ejection from the apex region of the wing, distance x_c indicates the location of the leading edge of the core from the apex of the wing. The completion of this ejection process corresponds to the attainment of maximum length of the core and abrupt onset of vortex breakdown; the distance of this breakdown position from the apex of the wing is designated as x_b.

It is important to distinguish here between the dynamic hysteresis loops of the type shown in Fig. 9, in contrast to static hysteresis that is represented by two different steady flow states at the same static angle of attack (Lawson[24]). Such hysteresis is characterized by a different value of x_b of the leading-edge vortices at the same value of α, depending upon the history of the (quasistatic) angle of attack α. It typically occurs for highly swept wings at value of α larger than those considered herein. No static hysteresis was observed over the range of wing and flow parameters of this investigation.

D. Hysteresis of Development and Breakdown of Core of Secondary Vortex

Up to this point, attention has been focused on the characteristics of the so-called primary vortex, i.e., the major vortex that is continuously fed by vorticity shed from the leading edge of the wing. In the case of flow past a stationary wing, there can exist secondary vortices between the primary vortex

and the leading edge of the wing (see Fig. 3). We focus here on the secondary vortex immediately adjacent to the leading edge of the wing, since its development and breakdown were found to be shifted in phase with respect to that of the primary vortex, as illustrated in Fig. 10. Over the relatively wide range of parameters investigated, and detailed in Sec. IVA, the following trend occurred consistently: onset of breakdown of the secondary vortex always precedes that of the primary one. As a consequence, immediately prior to the onset of breakdown of the primary vortex, there exists a region of reverse flow between the leading edge of the wing and the core of the primary vortex.

Hysteresis loops of this secondary vortex development and breakdown in relation to its primary counterpart are given in Fig. 10 for three different values of reduced frequency K. At the lowest reduced frequency $K=0.28$, the form of the secondary and primary vortex hysteresis loops is remarkably similar. However, there is reappearance and increase of the breakdown length x_b of the secondary vortex at lower values of α; this trend is accompanied by the tendency of the breakdown length of the primary vortex to increase at lower values of α.

At higher values of reduced frequency $K=0.76$ and 1.94, the formation of both the secondary and primary vortices is characterized by ejection of the leading edges of their cores from the apex region of the wing; the length of the ejected core

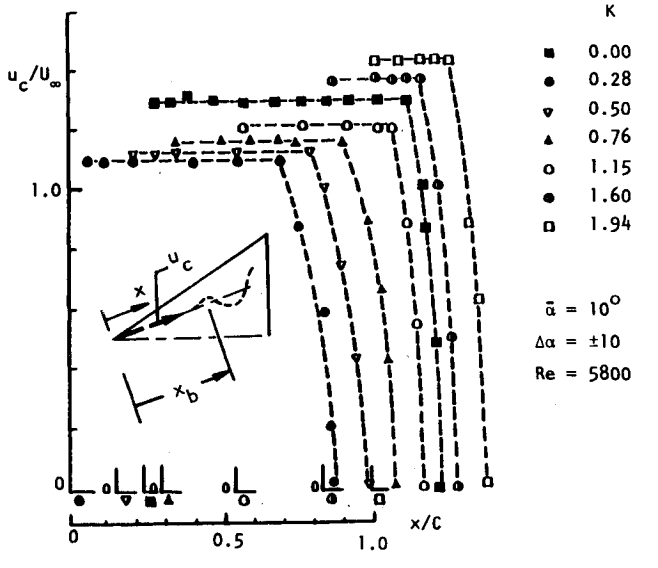

Fig. 11 Variation of axial velocity u_c along centerline of vortex core during vortex development of an oscillating delta wing.

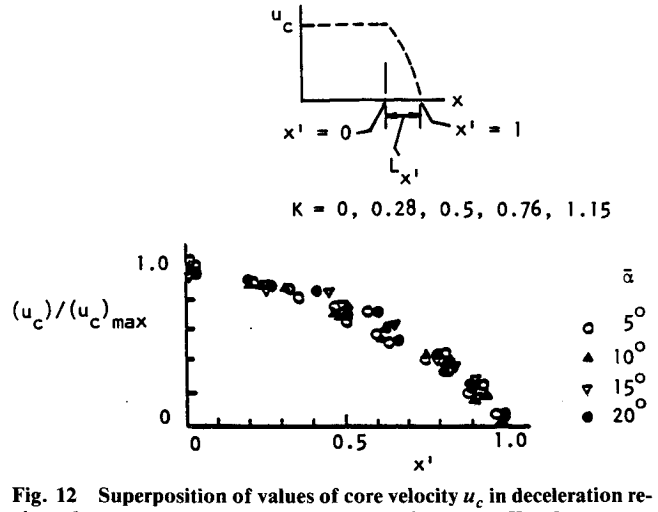

Fig. 12 Superposition of values of core velocity u_c in deceleration region of vortex core for a range of reduced frequency K and mean angle of attack α.

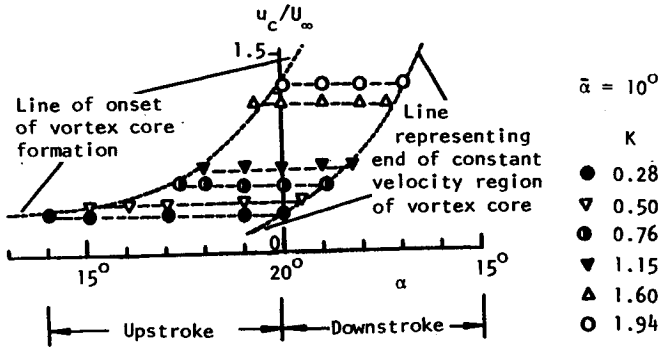

Fig. 13 Core velocity u_c variation as a function of instantaneous angle of attack α. (Only constant velocity region of core is plotted.)

is designated as x_c. For both vortices, when x_c reaches its maximum value, there is onset of vortex breakdown, whose position is given as x_b. Again, the maximum value of x_b for the secondary vortex is substantially smaller than its primary counterpart. The exception occurs at very high values of reduced frequency, represented by $K=1.94$. In this case, the very rapid development of the instability of the primary vortex precludes the large value of x_b; consequently, the maxima of x_b for both primary and secondary vortices are of the same order.

E. Velocity of Vortex Core

Particularly challenging is determination of the instantaneous velocity of the vortex core as a function of instantaneous angle of attack. The instantaneous axial velocity on the centerline of the core, designated as u_c, can be determined by tracking pulsed bubble markers; they were generated by use of the same visualization technique as described in Sec. II and shown in the core visualization of Secs. III and IV for which continuous, as opposed to pulsed, bubble generation was employed. The total uncertainty in determining u_c is $0.014U_\infty$. Velocity u_c was obtained as a function of streamwise distance from the apex of the wing for the range of mean angle of attack $\bar{\alpha}$ and reduced frequency K described in Sec. IVA. Figure 11 shows a representative family of curves for a mean angle of attack $\bar{\alpha}=10$ deg over a range of reduced frequency. Similar variations were obtained for $\bar{\alpha}=5$ and 15 deg.[22] Remarkable is the fact that the velocity u_c remains essentially constant with distance x until the abrupt onset of deceleration. The effect of increasing reduced frequency is to increase velocity u_c. However, comparison of the values of constant u_c for the oscillating wing ($K\neq 0$) with those of the stationary wing ($K=0$) at $\bar{\alpha}=10$ and 15 deg shows that motion of the wing can induce substantially smaller values of constant u_c.[22] All of the aforementioned trends must be interpreted in the context of the phase shift between the vortex development and the motion of the wing; this aspect will be addressed in Fig. 13.

The streamwise extent of the region of constant u_c decreases with increasing values of K. Correspondingly, the streamwise distance over which deceleration (decrease of the velocity u_c) occurs decreases with increasing K. Considering the range of mean angle of attack $\bar{\alpha}$ and reduced frequency K addressed in this investigation, it is possible to normalize the value of u_c by its maximum value $(u_c)_{max}$ at the onset of core deceleration, and the streamwise distance x by the distance $L_{x'}$, over which the core deceleration occurs. Such a normalization produces collapse of the data shown in Fig. 12. Note that $x'=0$ represents the onset of deceleration and $x'=1$ gives the location of the instantaneous stagnation condition $u_c=0$. The trend of the data corresponds to the velocity variation one would expect for stagnation flows. Keller et al.[25] have calculated the streamlines corresponding to the transition (breakdown) of a Rankine vortex for the case of steady flow. Their patterns clearly show the nature of the stagnation flow and the fact that

rapid deceleration of the core occurs over a very short streamwise distance of the order of the radius of the vortex core.

In the foregoing, we have considered the instantaneous core velocity u_c as a function of distance x from the apex of the wing, without regard for the instantaneous angle of attack α. That is, since the core develops along the wing, which is undergoing unsteady motion according to $\alpha(t)$, the instantaneous velocity u_c will be a function of α. Figure 13 shows plots of u_c/U_∞ vs α. Similar variations occur for other values of $\bar{\alpha}$.[22] For purposes of simplicity, only the constant velocity region of u_c is considered. In each plot, the dashed line located on the left-hand side of each diagram corresponds to that value of α at which there is onset of vortex core formation, while the dashed line on the right-hand side represents the end of the constant velocity region of the vortex core. Regions of upstroke and downstroke of the wing motion are also designated. Since the wing is driven in simple harmonic motion, the velocity of the apex of the wing is zero at the maximum angle of attack where it changes from upstroke to downstroke motion. Striking is the fact that the core velocity remains constant through the region where the wing velocity goes to zero. This observation again emphasizes the importance of considering the phase shift between the onset of vortex formation and its subsequent development relative to the instantaneous angle of attack of the wing.

V. Concluding Remarks

Flow past the leading edge of a stationary delta wing having moderate sweep angle generates a nonaxisymmetric primary vortex having a quasielliptical cross section; its shape and orientation vary with distance along the wing. Distributions of swirl angle of the vortex were determined by considering a series of streamlines emanating from various locations along the leading edge. The swirl-angle distribution is expressed as a function of 1) distance along the edge; 2) and radial distance from the center of the vortex. Irrespective of which interpretation is employed, the maximum values of swirl angle are within or somewhat below the ranges observed in tube flows by Garg and Leibovich[15] and Sarpkaya[20] for which breakdown in the spiral mode occurred. However, our maximum swirl angles are below those for which they observed breakdown in the bubble mode. These findings are consistent with our extensive flow visualization of the vortex breakdown, excerpts of which are given herein; only spiral-mode breakdown was observed. Finally, we note that the maximum swirl angle increases, as expected, with increasing angle of attack of the wing; this trend corresponds to upstream movement of the location of vortex breakdown.

For the pitching delta wing, the development of the vortex core in the vicinity of the apex shows two fundamental types of behavior, one occurring at low frequencies and the other at high frequencies of wing oscillation. Above a threshold value of excitation frequency, there occurs ejection of the leading edge of the core from the apex region in the downstream direction. Below this threshold, the origin of the vortex core gradually moves upstream towards the apex until the core is fully formed. The timing (or phasing) of both types of vortex development relative to the wing position is a strong function of reduced frequency. Even at low reduced frequencies, there is substantial phase shift between the development of the vortex core and the motion of the wing, relative to that which occurs on a statically displaced wing.

As a consequence of the phase shift associated with the vortex development, it is possible for the maximum length of the vortex to occur at or near the maximum angle of attack of the wing. Of course, this observation is in direct contrast to what is observed for the case of the stationary wing, namely, that the minimum length of the vortex core occurs at the maximum angle of attack. Presumably, this concept can be used to advantage in maneuvering of delta wings or control surfaces attached to such wings. It remains for further study to determine the relationship between the maximum values of lift and moment and the occurrence of maximum length of the vortex core.

The structure of the vortex core prior to, and at the onset of, vortex breakdown can take on a variety of forms, strongly dictated by the reduced frequency of the wing oscillation. At sufficiently low values of reduced frequency, the vortex breakdown occurs in the classical spiral mode, very similar to that observed on the corresponding stationary wing. However, at higher values of reduced frequency, there are a number of other modes of vortex breakdown that can compete with, or supersede, the classical spiral mode.

The phase shift between the occurrence of vortex breakdown and the instantaneous position of the wing can be expressed in terms of the location of breakdown x_b as a function of instantaneous angle of attack α. There occurs substantial hysteresis in the plot of x_b vs α, even at very low reduced frequencies of the order of $K=0.025$. Physically, this corresponds to a ratio of the wavelength $\lambda_e = f_e/U_\infty$ of the forcing to the chord C of the wing of the order of 10^{-2}. The direction of the hysteresis loops switches from clockwise to counterclockwise at sufficiently high values of reduced frequency. This switch is directly linked to the change in the nature of the vortex development; it corresponds to occurrence of the aforementioned threshold separating rapid ejection of the core from its gradual development. In the extreme case of high reduced frequency K, there exists no vortex core over a substantial portion of the oscillation cycle. In this limit, the vortex development is drastically shifted (in phase) relative to that occurring on the statically displaced wing.

To further characterize the development of the primary vortex, the instantaneous axial velocity (along the centerline of the vortex) was tracked while the wing was in motion. This velocity is remarkably constant until the onset of deceleration of the vortex core that eventually leads to vortex breakdown. The streamwise extent of this region of deceleration is of the order of one-tenth of the wing chord; it decreases with increasing values of reduced frequency. Over the range of reduced frequency and mean angle of attack examined, normalized distributions of core velocity vs distance along the deceleration zone suggest a universal distribution of axial core velocity characteristic of that in a steady stagnation flow.

Particularly remarkable is the fact that once the core development is initiated at a certain angle of attack in the oscillation cycle, the core (axial) velocity persists irrespective of the velocity of the apex of the wing. That is, since the wing is undergoing simple harmonic motion, the tip velocity at the apex goes on to zero when maximum angle of attack is achieved; yet the core velocity can remain constant through this region of zero tip velocity. This observation emphasizes the importance of the phase shift of the fluid motion relative to the wing motion. Further studies should address the issue of simultaneously measuring the instantaneous swirl velocity and the instantaneous radius of the core in order to fully characterize the core velocity field leading to breakdown.

There occur two secondary vortices between the leading edge of the wing and the primary vortex. The secondary vortex adjacent to the leading edge is fed by vorticity shed from the edge, while its inboard neighbor (located outboard of the primary vortex) is fed by vorticity from the wall boundary layer. This secondary vortex immediately adjacent to the leading edge undergoes a development and breakdown process similar to that of the primary vortex. However, the evolution of this secondary vortex is shifted in phase with respect to its primary counterpart; the breakdown of the secondary vortex always leads that of the primary vortex. As a consequence, there exists a region of reverse flow along the leading edge of the wing immediately prior to the onset of primary vortex breakdown. The general form of the hysteresis loops for the secondary vortex adjacent to the leading edge are very similar to those of its primary counterpart. Obviously, a complete picture of breakdown of the primary vortex requires knowledge of how the breakdown of the secondary vortices influences the instan-

taneous velocity distribution of the primary vortex; in turn this velocity field determines the criticality condition for onset of breakdown of the primary vortex.

Acknowledgments

The authors would like to express their appreciation for financial support from the Air Force Office of Scientific Research. Moreover, they benefitted from critiques by L. Carr, H. Helin, and J. McMichael during the course of this investigation.

References

[1]Lee, G. H., "Note on the Flow Past Delta Wing with Sharp Leading Edges," Aeronautical Research Council, Rept. and Memorandum 3070, Sept. 1958.

[2]Ornberg, H., "A Note on the Flow Around Delta Wings," Swedish TN K. T. H. Aero. TN 38, 1954.

[3]Elle, B. J., "An Investigation at Low Speed of the Flow Near the Apex of Delta Wings with Sharp Leading Edges," Aeronautical Research Council, Rept. and Memorandum 3176, 1958.

[4]Kuechemann, D., "On Nonlinear Lifting-Surface Theory for Wings of Small Aspect Ratio with Separation," Aeronautical Research Council, Rept. 17769, April, 1959.

[5]Kuechemann, D., "The Aerodynamic Design of Aircraft—An Introduction. Pt. V," Royal Airforce Establishment TM 1622, 1975.

[6]Hoeijmakers, H. W. M., "Computational Vortex Flow Aerodynamics," *Aerodynamics of Vortical Type Flows in Three Dimensions,* AGARD CP 342, 1983, pp. 18-1-18-35.

[7]Rizzi, A., Eriksson, L.-E., Schmidt, W., and Hitzel, S., "Numerical Solutions of the Euler Equations Simulating Vortex Flows Around Wings," *Aerodynamics of Vortical Type Flows in Three Dimensions,* AGARD CP 342, 1983, pp. 21-1-21-14.

[8]Woodson, S. H. and DeJarnette, S. R., "A Direct and Inverse Boundary Method for Subsonic Flow Over Delta Wings," *Vortex Flow Aerodynamics,* NASA Conference Publication 2416, Vol. 1, edited by J. F. Campbell, R. S. Osborn, and J. T. Foughner, 1986, pp. 115-134.

[9]Lambourne, N. C., Bryer, D. W., and Maybrey, J. F. N., "The Behavior of the Leading-Edge Vortices Over a Delta Wing Following Sudden Change of Incidence," Aeronautical Research Council Technical Rept. 3645, 1969.

[10]Gad-el-Hak, M. and Ho, C.-M., "The Pitching Delta Wing," *AIAA Journal,* Vol. 23, No. 11, 1985, pp. 1660-1665.

[11]Gad-el-Hak, M. and Ho, C.-M., "Unsteady Vortical Flow Around Three-Dimensional Lifting Surfaces," *AIAA Journal,* Vol. 24, May 1986, pp. 713-721.

[12]Wedemeyer, E., "Vortex Breakdown," AGARD Lecture Series No. 121, *High Angle of Attack Aerodynamics,* Dec. 1982, pp. 9-1-9-17.

[13]Atta, R. and Rockwell, D., "Hysteresis of Vortex Development and Breakdown on an Oscillating Delta Wing," *AIAA Journal,* Vol. 25, No. 11, 1987, pp. 1512-1513.

[14]Sarpkaya, T., "Effect of Adverse Pressure Gradient on Vortex Breakdown," *AIAA Journal,* Vol. 12, No. 5, 1974, pp. 602-607.

[15]Garg, A. K. and Leibovich, S., "Spectral Characteristics of Vortex Breakdown Flowfield," *Physics of Fluids,* Vol. 22, No. 11, 1979, pp. 2053-2064.

[16]Escudier, N. P., "Confined Vortices in Flow Machinery," *Annual Review of Fluid Mechanics,* Vol. 19, 1987, pp. 27-52.

[17]Leibovich, S., "Structure of Vortex Breakdown," *Annual Review of Fluid Mechanics,* Vol. 10, 1978, pp. 221-246.

[18]Leibovich, S., "Vortex Stability and Breakdown: Survey and Extension," *AIAA Journal,* Vol. 22, No. 9, 1984, pp. 1192-1206.

[19]Lambourne, N. C., "The Breakdown of Certain Types of Vortex," Aeronautical Research Council Current Paper 915, 1965.

[20]Sarpkaya, T., "On Stationary and Travelling Vortex Breakdown," *Journal of Fluid Mechanics,* Vol. 45, Pt. 3, 1971, pp. 549-559.

[21]Faler, T. H. and Leibovich, S., "Disrupted States of Vortex Flow and Vortex Breakdown," *Physics of Fluids,* Vol. 20, Sept. 1977, pp. 1385-1400.

[22]Atta, R., "Unsteady Structure of Flow Past a Pitching Delta Wing," Ph.D. Thesis, Dept. of Mechanical Engineering and Mechanics, Lehigh Univ., Bethlehem, PA, 1987.

[23]Reynolds, G. A. and Abtahi, A. A., "Instabilities in Leading-Edge Vortex Development," AIAA Paper 87-2424, Aug. 1987.

[24]Lawson, M. V., "Some Experiments on the Vortex Breakdown," *Journal of the Royal Aeronautical Society,* Vol. 68, May 1964, pp. 343-346.

[25]Keller, J. J., Egli, W., and Exley, J., "Force- and Loss-Free Transitions Between Vortex Flow States," *Studies of Vortex Dominated Flows,* edited by M. Y. Hussani and M. B. Salas, Springer-Verlag, 1987, pp. 53-75.